Effect of Salt Concentration on Uniform Hydrogen Sulfide Corrosion Rate of Pipeline Steel

Fazlollah Madani Sani, Bruce Brown, Srdjan Nesic
Institute for Corrosion and Multiphase Technology, Ohio University
342 W State Street
Athens, Ohio, 45701
USA

ABSTRACT

Large amounts of water can be produced during the production of hydrocarbons from underground reservoirs. Salts are always dissolved in these produced waters. The concentration of dissolved salts can be as high as 400 g/l. For the first time, the effect of salt concentration on uniform hydrogen sulfide (H_2S) corrosion of carbon steel in aqueous solutions is studied. Linear polarization resistance (LPR) and potentiodynamic polarization (PD) experiments were conducted in aqueous solutions at 20°C and pH 5.00 saturated with an H_2S/N_2 gas mixture with a total pressure of 1 bar and H_2S concentration of 100 ppm(v). Two NaCl concentrations were tested: 1 and 20 wt.%. A rotating cylinder electrode with a rotational speed of 1000 rpm was used as the specimen. LPR corrosion rates indicated that H_2S corrosion rate decreased with increasing salt concentration. PD results showed that the corrosion process was under mixed control. Increasing salt concentration retarded both the anodic and the cathodic reactions, and thereby, decreased the rate of uniform H_2S corrosion.

Keywords: hydrogen sulfide corrosion, pipeline corrosion, salt concentration, salinity, rotating disk electrode (RDE), produced water

INTRODUCTION

Large amounts of water can be produced during extraction of hydrocarbons from underground reservoirs.[1] It is well understood that produced waters usually contain high amounts of dissolved salts, up to 28 wt.%.[2] In addition to salts, dissolved corrosive gases (CO_2 and H_2S) are present in produced water, which make the mixture a complex corrosive environment for metallic parts and equipment used throughout the production process.

Internal H_2S corrosion of carbon steel tubulars often occurs in the oil and gas industry, particularly when drilling deeper to search for new oil and gas reservoirs.[3,4] In contrast to CO_2 corrosion, a limited number of studies exist for H_2S corrosion. And, to the best knowledge of the authors, no study has been done on the effect of salt concentration on uniform H_2S corrosion. It is necessary to understand H_2S corrosion mechanisms in high saline solutions to develop a correct corrosion prediction. For the first time, the effect of salt concentration on uniform H_2S corrosion of carbon steel in aqueous solutions is presented as part of a wider mechanistic study.

This work, as a small part of a larger joint-industrial project (JIP) focused on corrosion mechanisms related to the internal CO_2/H_2S corrosion of pipeline-grade carbon steel, covers the effect of salt concentration on uniform H_2S corrosion in acidic media. The data presented in this article is used in development of a corrosion-rate-prediction model as one of the goals of the JIP.

In this paper, the effect of NaCl concentration on corrosion behavior of X65 carbon steel was investigated by performing electrochemical experiments in aqueous solutions with two NaCl concentrations at $20^{\circ}C$, 1 bar total pressure, pH 5.00, and 100 ppm H_2S concentration in the gas phase.

EXPERIMENTAL PROCEDURE

Two objectives were followed in this study. First and foremost, to study the effect of salt concentration on H_2S corrosion at low H_2S concentrations. Second, to build experience and confidence in safely working with the poisonous H_2S gas for experiments using H_2S gas at a partial pressure of ~1 bar. The experiments in this part of study were done at pH 5.00 to intensify the contribution of the H_2S buffering effect in the H_2S corrosion process. Bulk solution pH was kept constant at pH 5.00 for experiments at all salt concentrations, so that the only parameter changed in the experiments was NaCl concentration. This testing methodology allowed a better understanding of the effect of salt concentration on the H_2S corrosion process.

Setup and apparatus

Experiments were conducted at $20^{\circ}C$, 1 bar total pressure for two NaCl concentrations of 1 and 20 wt.% in a 2-liter glass cell. The temperature of $20^{\circ}C$ was chosen identical to that in CO_2 experiments to allow comparing the corrosion rate measurements in H_2S- and CO_2-saturated solutions[†]. The schematic of the experimental apparatus used in this part is shown in Figure 1.

The gas atmosphere exposed to the solution was an H_2S/N_2 mixture with 100 ppm(v) H_2S gas balanced with N_2 gas. 100 ppm(v) H_2S gas concentration is equivalent to 10^{-4} bar $H_2S_{(g)}$. The H_2S and N_2 gases were mixed, and their ratio was adjusted by using a double-column rotameter. The outlet gas mixture from the glass cell was passed through a saturated NaOH solution followed by an activated carbon-containing flask to scrub H_2S gas from the gas mixture. The scrubbed gas was then sent to a combustion chamber with excess air where the remaining H_2S in the gas stream was converted to sulfur dioxide (SO_2). It has been determined that the combustion process is near 100% conversion and no detectable H_2S remains in the effluent gas.

To adjust the solution temperature to $20^{\circ}C$, water was circulated from an industrial chiller through a copper coil around the glass cell to cool down the solution temperature. In combination with the cooling coil and insulation around the cell, a hot plate was used continuously to balance the temperature at $20 \pm 0.5^{\circ}C$.

For each experiment, the desired amount of NaCl was mixed with deionized water (conductivity < 1 μS/cm) in the glass cell. Then, the solution was sparged with the H_2S/N_2 gas mixture for at least 3 h, while being stirred by a magnetic stirrer. The 3 h was identified experimentally as the least amount of time needed to drop the concentration of dissolved oxygen in the solution (~ 2 liter) to less than 10 ppb and saturate the solution with the gas mixture. The dissolved oxygen was measured during the experiments with an Orbisphere[‡] 410 oxygen meter connected to the gas outlet to assure that the oxygen level in the solution was less than 10 ppb. The solution pH was frequently monitored from the beginning
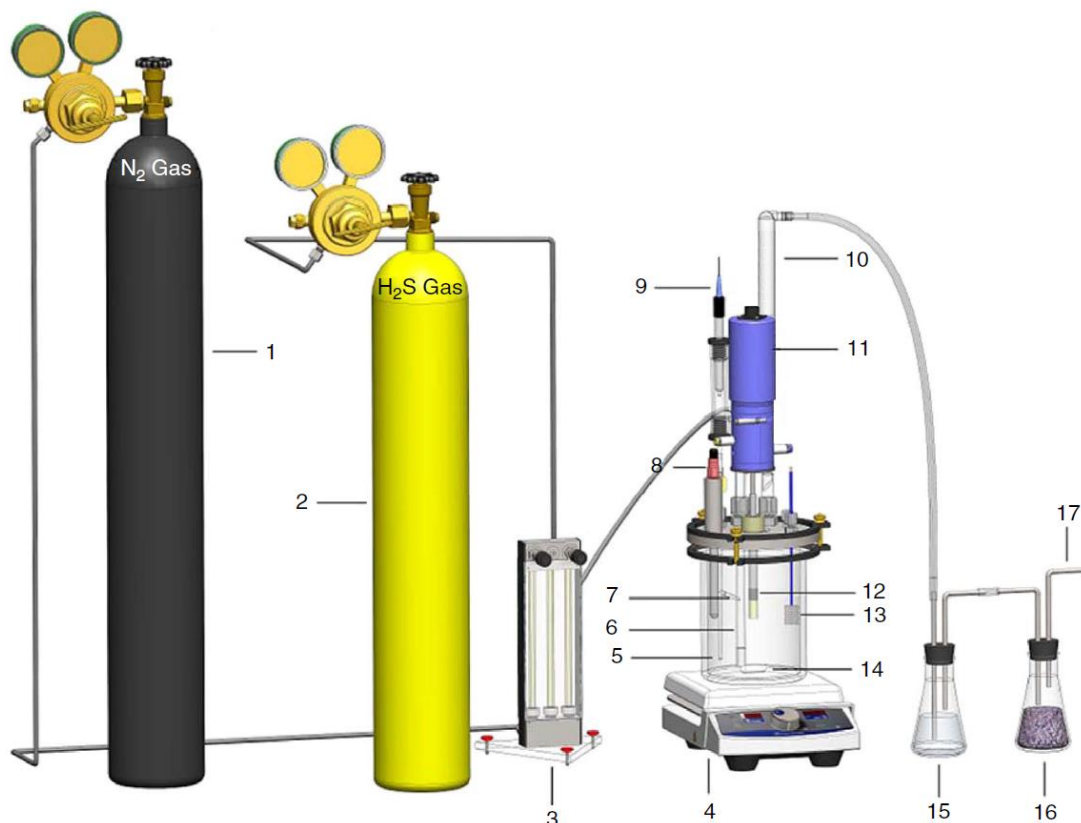

[†] The comparison is not the focus of this study.

[‡] Trade name.

to the end of each experiment. The solution was identified saturated with the gas mixture when solution pH stayed stable ($\Delta pH < 0.01$) for at least 15 min. Double-junction pH probes suitable for concentrated brines and resistant to H_2S were used for the pH measurements.

Figure 1. The schematic of the experimental apparatus used for RCE H_2S experiments at pH 5.00 and 100 ppm $H_2S(g)$. The assigned numbers represent: (1) N_2 gas cylinder, (2) H_2S gas cylinder, (3) double-column rotameter, (4) hot plate, (5) thermocouple, (6) gas inlet, (7) Luggin capillary, (8) pH-electrode, (9) reference electrode, (10) gas outlet from the cell, (11) motor, (12) rotating cylinder electrode, (13) platinum coated counter electrode, (14) stir bar, (15) sodium hydroxide solution, (16) activated carbon scrubber, (17) gas outlet to the combustion chamber.

Once a stable pH was attained, the solution pH was adjusted to pH 5.00 by injecting deaerated HCl 0.01 M to the solution. To make sure that solution pH stayed fixed at 5.00, the solution was sparged with the gas mixture for another 0.5 h prior to inserting the specimen into the solution and before beginning the electrochemical measurements. The magnetic stirrer was stopped throughout the electrochemical measurements.

Material tested

The specimen material was API 5L X65 pipeline grade carbon steel.[5] The chemical composition of this X65 steel is defined in Table 1. The carbon steel microstructure (not shown here) is a uniform, fine structure of pearlite in a ferrite matrix. The RCE specimen used have an outer diameter of 12 mm, a length of 14 mm, and an outer surface area of 5.4 cm². The cell volume to specimen surface area ratio in the experiments was approximately 370 cm³/cm², which was much larger than the average minimum ratio of 30 cm³/cm² suggested by ASTM G31.[6] Prior to each experiment, the specimen was sequentially wet polished with 80-, 240-, 400- and 600-grit abrasive papers. Then, the specimen was ultrasonically cleaned in an isopropanol bath for 3 min and dried in a cool N_2 gas stream. The RCE specimen was carefully mounted onto the RCE shaft without touching its surface and the whole assembly was

transferred into the glass cell. The RCE assembly was rotated at 1000 rpm, which simulates the mass transfer conditions in a 10 cm ID pipe with an average flow velocity of 1 m/s.[7]

Table 1. Chemical composition of the experimental carbon steel (API 5L X65) (in wt.%).

Al	As	C	Co	Cr	Cu	Mn	Mo	Nb	Ni
0.028	0.008	0.05	<0.001	0.252	0.173	1.51	0.092	0.034	0.291
P	**S**	**Sb**	**Si**	**Sn**	**Ti**	**V**	**Zr**	**Fe**	
0.004	<0.001	<0.001	0.167	0.002	0.012	0.04	<0.001	balance	

Electrochemical measurements

In each experiment, EIS, LPR, and PD sweeps were performed, using the same specimen. First, the EIS was done to measure the solution resistance. Then LPR was conducted for the corrosion rate measurements to identify the overall effect of salt concentration on the H_2S corrosion rate. Finally, PD sweeps were obtained to investigate how individual reaction mechanisms underlying H_2S corrosion are affected by salt concentration. For each NaCl concentration, the experiments were repeated two times.

The LPR technique was performed using a three-electrode setup as shown in Figure 1, using a potential range from -5 mV to +5 mV vs. OCP with a scan rate of 0.125 mV/s. The RCE acted as the working electrode. A saturated Ag/AgCl reference electrode connected to a Luggin capillary served as the reference electrode and a platinized titanium mesh (20 mm × 30 mm) was used as the counter electrode to complete the three-electrode setup. The duration of each LPR measurement was 80 sec. The average Stern-Geary constant (B) for converting the measured polarization resistance into the corrosion rate was determined to be around 18.7 mV/dec. This was done by fitting the PD sweeps via an electrochemical model.[8] The measured polarization resistance values were corrected for the solution resistance, which was measured by EIS. EIS was done prior to each LPR measurement at OCP with the same electrode setup as for LPR in a frequency range of 10000–0.1 Hz with a peak-to-peak AC voltage amplitude of 10 mV.

For the PD sweep measurements, before starting to sweep the potential, the open circuit potential (OCP) was monitored to ensure having a stable OCP value ($\Delta_{OCP} < 2$ mV/min). The PD sweep experiments were carried out according to the following steps: (1) a cathodic sweep starting from the OCP toward more negative potentials up to -1 V vs. OCP; (2) wait for the OCP to return near its initial value—within a few mV (this took about 1 h); (3) an anodic sweep starting from the OCP to more positive potentials up to 0.35 V vs. OCP. The PD sweep scan rate was 0.125 mV/s. All the PD sweeps were corrected for the solution resistance obtained by EIS. A Gamry potentiostat Reference 600[§] was used for all the electrochemical measurements. Each full set of electrochemical measurements required about 6 h. During each experiment, the increase in the solution pH was less than 0.05 pH units for all NaCl concentrations.

pH measurements

Figure 2 shows the autogenous pH of solution before pH adjustment for the 1 wt.% and 20 wt.% NaCl concentration solutions sparged with an H_2S/N_2 gas mixture at 100 ppm H_2S. The purpose of the dashed line is to just show the trend. The autogenous pH of solution increased with increasing NaCl concentration. The first speculation is that increasing salt concentration decreased H_2S solubility (the
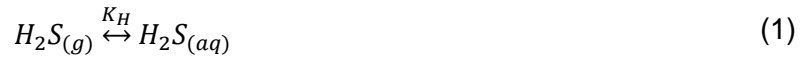

[§] Trade Name

salting out effect), and therefore pH increased. However, Madani Sani *et al.*[9] showed that it is the activity of dissolved gas and not its concentration (*i.e.*, H₂S solubility) that is linked to pH.

Since the experiments were carried out in an open system at a constant partial pressure of 100 ppm $H_2S_{(g)}$ for both NaCl concentrations, *i.e.*, continuous supply of $H_2S_{(g)}$ throughout the experiments, the fugacity of $H_2S_{(g)}$ ($f_{H_2S_{(g)}}$) was constant and the same for both NaCl concentrations. At a constant temperature and a constant partial pressure, the H₂S solubility equilibrium constant (K_H in Reaction (1)) is constant. Therefore, activity of $H_2S_{(aq)}$ ($a_{H_2S_{(aq)}}$) was constant and the same for both NaCl concentrations, following the equilibrium Equation (2). On the other hand, the equilibrium Equation (4) for the H₂S dissociation Reaction (3) shows that $a_{H^+_{(aq)}}$, an indication of solution pH ($= -\log_{10}(a_{H^+_{(aq)}})$), is associated with $a_{H_2S_{(aq)}}$ and not H₂S concentration ($c_{H_2S_{(aq)}}$). Therefore, $c_{H_2S_{(aq)}}$ decrease with increasing NaCl concentration cannot be the reason for the increase in solution pH.

$$H_2S_{(g)} \overset{K_H}{\leftrightarrow} H_2S_{(aq)} \tag{1}$$

$$K_H = \frac{a_{H_2S_{(aq)}}}{f_{H_2S_{(g)}}} \tag{2}$$

$$H_2S_{(aq)} \overset{K_1}{\leftrightarrow} HS^-_{(aq)} + H^+_{(aq)} \tag{3}$$

$$K_1 = \frac{a_{H^+_{(aq)}} a_{HS^-_{(aq)}}}{a_{H_2S_{(aq)}}} \tag{4}$$

As mentioned by Madani Sani *et al.*[9] for the CO₂ saturated solutions, and it is expected to be the same here, the changes in the autogenous pH of solution with salt concentration is due to variations in the interactions between different species in the solution that alter the H⁺ ion activity coefficient.

However, the observed increasing trend in pH is opposite to the trend observed for autogenous pH with respect to NaCl concentration in CO₂-saturated solutions.[9–14] Experiments with pure H₂S gas at different NaCl concentrations (results will be presented in future publications) showed a decreasing trend in pH with increasing NaCl concentration, similar to pH measurements in CO₂-satuarted solutions. Therefore, it can be speculated that the presence of N₂ gas and its effect on interspecies interactions in the solution caused the increase in pH with increasing NaCl concentration. The mixed solvent electrolyte (MSE) speciation equilibrium model[15] was not able to capture this unexpected trend for autogenous pH in 100 ppm H₂S(g) mixed with N₂ gas and predicts a declining trend with increasing NaCl concentration: 7.14 and 5.73 at 1 and 20 wt.% NaCl concentrations, respectively. Further investigations are required.
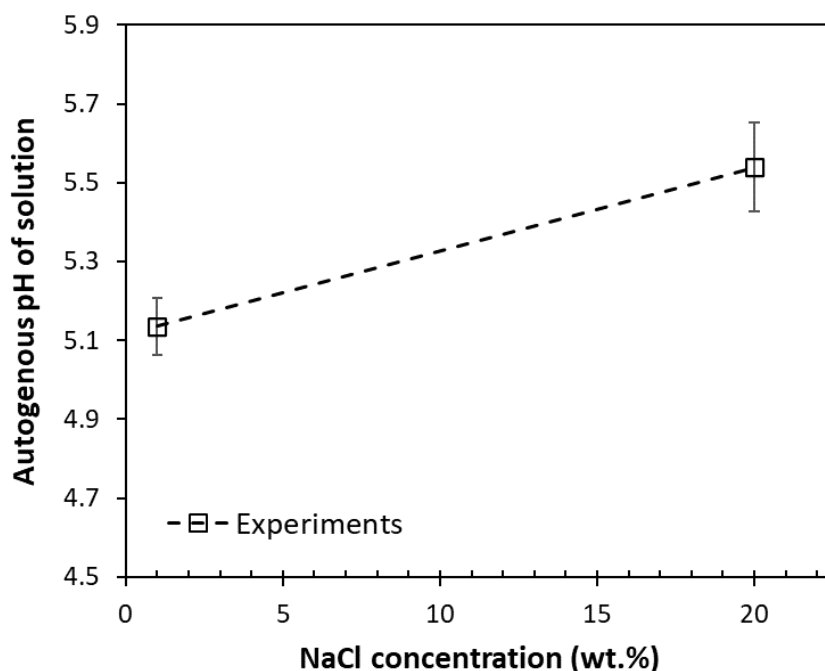
Figure 2. Autogenous pH of aqueous NaCl solutions at 20°C, and 1 bar total pressure saturated with a H_2S/N_2 gas mixture containing 100 ppm $H_2S_{(g)}$. The error bars represent the minimum and maximum values obtained in two repeated experiments.

Experimental conditions

A summary of the experimental conditions is listed in Table 2.

Table 2. The experimental conditions for studying the effect of salt concentration on uniform H_2S corrosion of carbon steel.

| Parameter	Description
Specimen material	X65 carbon steel
Specimen type	RCE
RCE rotational speed (rpm)	1000 ± 2
Temperature (ºC)	20.0 ± 0.5
Total pressure (bar)	1
Sparging gas	H_2S/N_2 mixture
H_2S partial pressure (bar)	10^{-4}
NaCl concentration (wt.%)	1 and 20
pH	5.00 ± 0.02

Results and Discussion

Corrosion rate measurements

Figure 3 shows the corrosion rate results obtained by LPR and PD sweep measurements at 100 ppm $H_2S_{(g)}$ and two NaCl concentrations. The corrosion rate values measured with both techniques were almost the same, indicating the accuracy of measurements and the reliability of the conclusions. The H_2S

corrosion rate decreased when NaCl concentration was increased from 1 wt.% to 20 wt.%. This agrees very well with the effect of salt concentration on uniform CO_2 corrosion rate reported elsewhere.[9,14] The decrease in H_2S corrosion rate with increasing NaCl concentration can be explained by analyzing the PD sweeps.
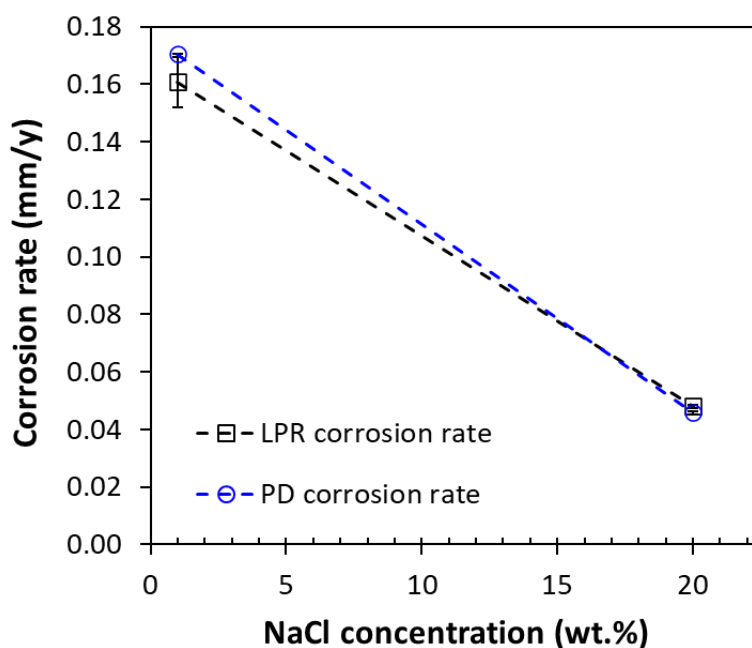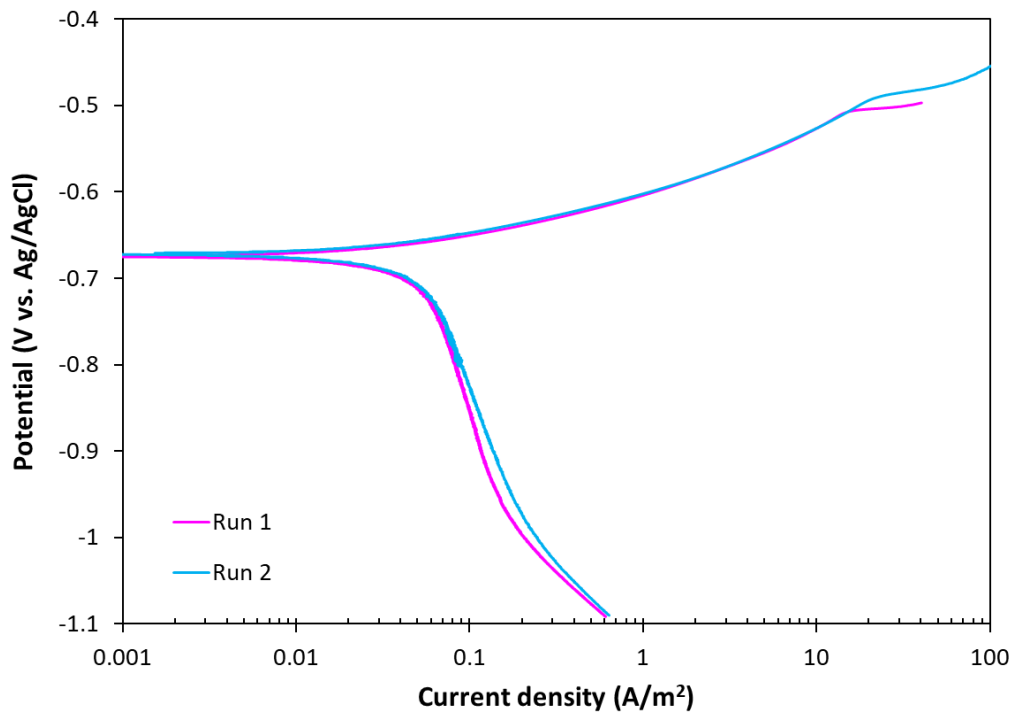

Figure 3. The variation in the corrosion rate with NaCl concentration for X65 RCE specimen (1000 rpm) exposed to aqueous solutions at 20°C and pH 5.00 saturated with 100 ppm $H_2S_{(g)}$ at 1 bar total pressure.

Potentiodynamic polarization sweep analysis

The PD sweeps from two separate runs at 20 wt.% NaCl, 20°C, pH 5.00 and 100 ppm $H_2S_{(g)}$ are presented in Figure 4 as an example to confirm that the PD sweep measurements were repeatable. Therefore, the conclusions based on the PD sweeps can be trusted.

Figure 5 shows the PD sweeps for 1 wt.% and 20 wt.% NaCl concentrations at 20°C, pH 5.00 and 100 ppm $H_2S_{(g)}$. The potential values are corrected for the solution resistance (iR drop) in all the given sweeps. Both anodic and cathodic branches of the sweeps changed with increasing NaCl concentration. The anodic dissolution of iron in the active region and the H^+ ion reduction reaction in the charge transfer region were retarded with increasing NaCl concentration. There was a decrease in the H^+ ion reduction limiting current density (i_{Lim}) when NaCl concentration was increased. The water reduction reaction seems to be unaffected by the higher NaCl concentration.

Figure 4. Potentiodynamic sweeps from two separate runs for X65 carbon steel RCE with a rotational speed of 1000 rpm exposed to a solution, at 20°C, pH 5.00, and 20 wt.% NaCl, saturated with 100 ppm $H_2S_{(g)}$ at 1 bar total pressure.
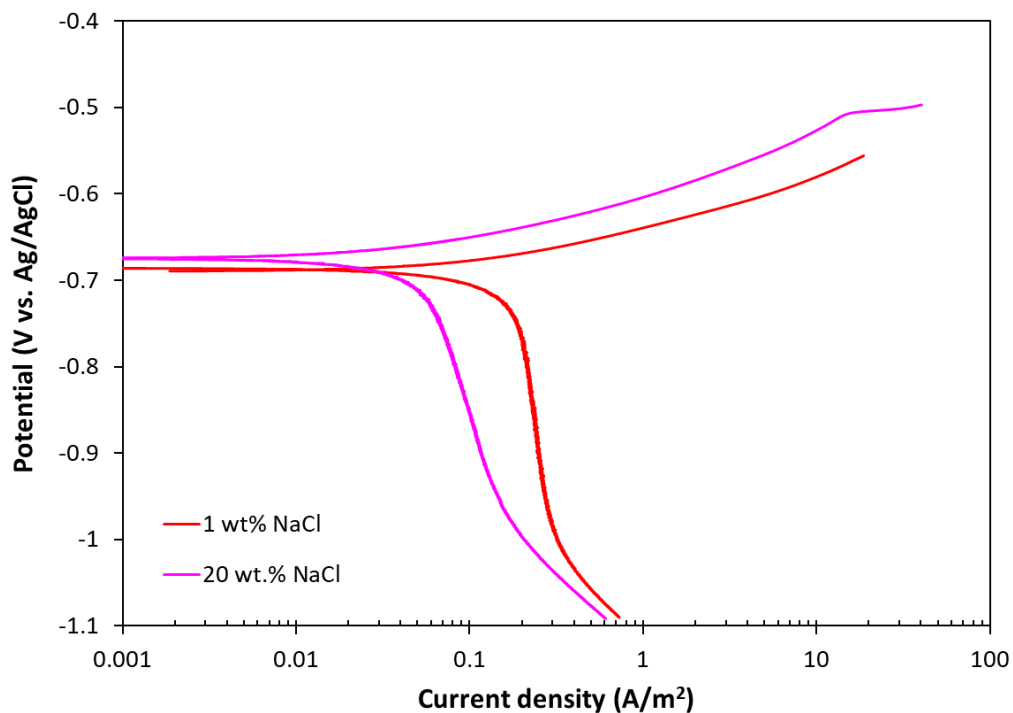
Figure 5. Potentiodynamic sweeps for X65 carbon steel RCE with a rotational speed of 1000 rpm exposed to aqueous NaCl solutions, at 20°C and pH 5.00, saturated with 100 ppm $H_2S_{(g)}$ at 1 bar total pressure.

To quantify the effect of NaCl concentration on each of the parameters mentioned above, the kinetic features of the PD sweeps were extracted by finding the best fit calculated by a simple electrochemical model based on the experimental sweeps. An activation energy of 59860 J/mol for the H^+ ion reduction reaction, 24809 J/mol for the H_2O reduction reaction, and 25398 J/mol for the Fe oxidation reaction were used. A reversible potential of -0.685[**] V vs. Ag/AgCl was used for all three reactions. The reference temperature was 20°C.

The electron transfer coefficients for the H^+ ion reduction reaction (α_{H^+}) and the Fe oxidation reaction in the active region (α_{Fe}) at 20°C, pH 5.00, 100 ppm H_2S and NaCl concentrations of 1 wt.% and 20 wt.% are presented in Table 3. α_{H^+} values are the same as the theoretical value of 0.5, commonly considered for the hydrogen evolution reaction on an iron surface.[17] Since α_{H^+} did not change with varying NaCl concentration, it can be concluded that the mechanism of hydrogen evolution under the experimental conditions used in this set of experiments was not affected by salt concentration.

Table 3. The average electron transfer coefficients for H⁺ reduction reaction (α_{H^+}) and Fe oxidation (α_{Fe}) for the RCE (1000 rpm) H₂S experiments in aqueous NaCl solutions, at 20°C and pH 5.00, saturated with 100 ppm H₂S₍g₎ at 1 bar total pressure.[8]

NaCl concentration (wt.%)	1	20
α_{H^+}	0.50 ± 0.02	0.50 ± 02
Cathodic Tafel slope (mV/dec)	116 ± 4	116 ± 4
α_{Fe}	1.05 ± 0.02	1.20 ± 02
Anodic Tafel slope (mV/dec)	55 ± 1	48 ± 1

The α_{Fe} values are in the same range as 1.18 reported by Chin and Nobe [18] for dissolution of iron in acidic chloride media. There was an increase in α_{Fe} with increasing NaCl concentration from 1 wt.% to 20 wt.%. However, this increase is in the range of the experimental error and more NaCl concentrations need to be examined to be able to comment with confidence about any possible change in the mechanism of active dissolution of iron. It is expected that, similarly to CO_2 corrosion[9], there was no change in the iron dissolution mechanism in the active region in the presence of 100 ppm $H_2S_{(g)}$ with the change in salt concentration.

Table 4 presents the reference current densities for the H^+ ion reduction reaction (i_{o,H^+}), the iron dissolution reaction ($i_{o,Fe}$), and i_{Lim} for 1 wt.% and 20 wt.% NaCl concentrations at 20°C, pH 5.00 and 100 ppm $H_2S_{(g)}$ as determined by modeling the PD sweeps. The i_o is an indication of the rate of an electrochemical reaction. The i_o and the rate of the electrochemical reaction have a direct relationship. The i_{o,H^+} decreased when NaCl concentration was increased from 1 wt.% to 20 wt.%. This agrees well with the results reported for CO_2 corrosion.[9,14] The decrease in i_{o,H^+} with increasing NaCl concentration is related to the adsorption of Cl^- ions on the metal surface which interferes with the H^+ ion reduction reaction.[19] A reason for the decreasing trend seen for the corrosion rates in Figure 3 could be the decrease in i_{o,H^+}.

[**] The reversible potential of X65 carbon steel at standard conditions

Table 4. The cathodic limiting current density (i_{Lim}), the H⁺ reduction reference current density (i_{o,H^+}) and the Fe oxidation reference current density ($i_{o,Fe}$) for X65 carbon steel RCE with a rotational speed of 1000 rpm exposed to aqueous NaCl solutions, at 20°C and pH 5.00, saturated with 100 ppm $H_2S_{(g)}$ at 1 bar total pressure.

NaCl concentration (wt.%)	1	20
i_{o,H^+} (A/m²)	0.380	0.0875
i_{Lim} (A/m²)	0.233	0.087
$i_{o,Fe}$ (A/m²)	0.160	0.023

The $i_{o,Fe}$ decreased with increasing NaCl concentration from 1 wt.% to 20 wt.%, which means that the rate of anodic dissolution of Fe in the active region decreased at higher NaCl concentrations. This is identical to the results for changes in $i_{o,Fe}$ with NaCl concentrations greater than ~ 1 wt.% in CO_2 corrosion.[9] Hence, $i_{o,Fe}$ variation with NaCl concentration is possibly another reason for the decrease in the H₂S corrosion rate when NaCl concentration was increased from 1 wt.% to 20 wt.%.

The most noticeable change in the PD sweeps in Figure 5 with NaCl concentration was for i_{Lim}. In H₂S corrosion, i_{Lim} is an indication of the rate of the H⁺ ion reduction reaction that is controlled by the relatively slow rate of $H_2S_{(aq)}$ dissociation reaction coupled with the rate of the mass transfer of species to the metal surface. Table 4 shows that i_{Lim} decreased with increasing NaCl concentration from 1 wt.% to 20 wt.%. In H₂S corrosion, i_{Lim} depends on a_{H^+} and a_{H_2S}. The experiments were carried out in an open system (*i.e.*, a continuous supply of H₂S gas). Therefore, a_{H_2S} was constant for both NaCl concentrations. a_{H^+} was constant for both NaCl concentrations because the solution pH was adjusted at 5.00 in the experiments. Consequently, a_{H^+} and a_{H_2S} cannot be the reason for the decrease in i_{Lim} with NaCl concentration. i_{Lim} also depends on diffusion coefficients of H⁺ ion and H₂S as well as their activity coefficients. Out of these parameters, the contribution of H⁺ diffusion coefficient and its activity coefficient in the total i_{Lim} value is dominant. The i_{Lim} is directly related to H⁺ ion diffusion coefficient and inversely depends on H⁺ ion activity coefficient. The decreasing trend for i_{Lim} when NaCl increased from 1 wt.% to 20 wt.% is primarily due to the increase in H⁺ ion activity coefficients[9] as well as the decrease in the diffusion coefficient of H⁺ ion.[20,21] The decrease in i_{Lim} with NaCl concentration can be an additional reason for the decreasing trend seen for the H₂S corrosion rate in Figure 3.

Three possible reasons have been mentioned for the decrease in the H₂S corrosion rate at 20°C, pH 5.00 and 100 ppm $H_2S_{(g)}$ when NaCl concentration increased from 1 wt.% to 20 wt.%: the decreases in i_{o,H^+}, $i_{o,Fe}$, and i_{Lim} with increasing NaCl concentration. To understand which of these three parameters influences the H₂S corrosion process to a greater extent at the experimental conditions, the Evans diagram is used.

Review of the H₂S corrosion mechanism using the Evans diagram

The main electrochemical reactions underlying aqueous H₂S corrosion of mild steel under the experimental conditions of this study are active dissolution of iron:

$$Fe \rightarrow Fe^{2+} + 2e^- \tag{5}$$

and reduction of hydrogen ions:

$$2H^+ + 2e^- \rightarrow H_2 \tag{6}$$

Figure 6 illustrates the Evans diagrams based on the above reactions for 1 wt.% and 20 wt.% NaCl concentrations at the experimental conditions used in this study. For both NaCl concentrations, the corrosion process was under mixed control. This indicates that the rate of the H₂S corrosion process was controlled by both charge transfer processes as well as i_{Lim}. The reason for the decrease in the H₂S corrosion rate in the NaCl concentration range of 1 wt.% to 20 wt.% was due to retardation of both iron dissolution reaction and H⁺ ion reduction reaction in the charge transfer regions as well as the decrease in i_{Lim}.

Additionally, since the difference between i_{Lim} and i_{Corr} is smaller for 1 wt.% NaCl compared to that for 20 wt.% NaCl, the contribution of i_{Lim} in the overall H₂S corrosion rate was larger at 1 wt.% NaCl. This shows that under the experimental conditions of this study, increasing NaCl concentration slowed down the charge transfer processes more than the rate of parameters controlling i_{Lim}.
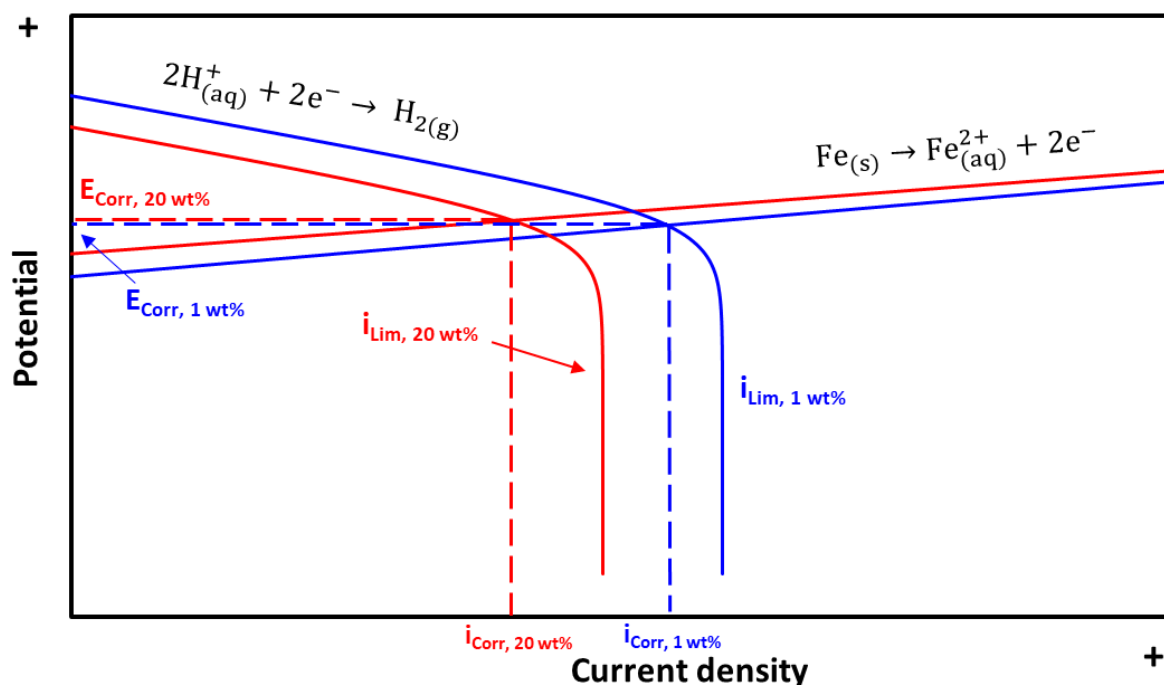

Figure 6. The Evans diagrams for the effect of NaCl concentration on uniform H₂S corrosion of X65 RCE with a rotational speed of 1000 rpm exposed to aqueous NaCl solutions, at 20°C and pH 5.00, saturated with 100 ppm H₂S(g) at 1 bar total pressure. E_{corr} is the corrosion potential (OPC), i_{corr} is the corrosion current density (blue: 1 wt.% NaCl, and red: 20 wt.% NaCl).

CONCLUSIONS

Experiments were carried out to understand the effect of salt concentration on aqueous uniform H₂S corrosion of carbon steel at low H₂S(g) concentrations. The main conclusions found, when NaCl concentration increased from 1 wt.% to 20 wt.%, are as follows:
1. The autogenous pH of solution increased for a solution sparged with an H₂S/N₂ gas mixture with 100 ppm H₂S. The increase was attributed to the unaccounted effect of N₂ gas. Further investigations are recommended on this subject.
2. The uniform H₂S corrosion rate decreased.

3. Analysis of PD sweeps indicated that the decrease in the H₂S corrosion rate was due to retardation of both iron dissolution and H⁺ ion reduction reactions in the charge transfer regions as well as the decrease in i_{Lim}. At 1 wt.% NaCl, i_{Lim} and at 20 wt.% NaCl charge transfer processes were dominant in the overall H₂S corrosion rate.
4. Evans diagrams showed that salt concentration influences the charge transfer processes more than i_{Lim} in the H₂S corrosion process under the experimental conditions.

ACKNOWLEDGEMENTS

REFERENCES

1 E. T. Igunnu and G. Z. Chen: 'Produced water treatment technologies', *Int. J. Low-Carbon Technol.*, 2014, 9, 157–177.
2 G. N. Breit: 'USGS Produced Waters Database', 2002, U.S. Department of the Interior.
3 Hart Energy and MathPro Inc.: 'Technical and economic analysis of the transition to ultra-low sulfur fuels in Brazil, China, India, and Mexico', 2012, International Council on Clean Transportation.
4 D. Chaudhuri and S. Oruganti: *Digit. Refin.*, 2018, No. 1001507.
5 F. Madani Sani, A. Afshar and M. Mohammadi: 'Evaluation of the simultaneous effects of sulfate reducing bacteria, soil type and moisture content on corrosion behavior of buried carbon steel API 5L X65', *Int. J. Electrochem. Sci.*, 2016, 11, 3887–3907.
6 ASTM International J01.01 Subcommittee: 'Guide for laboratory immersion corrosion testing of metals', 2004, ASTM International.
7 D. C. Silverman: 'Technical note: on estimating conditions for simulating velocity-sensitive corrosion in the rotating cylinder electrode', *CORROSION*, 1999, 55, 1115–1118.
8 S. Nesic, J. Postlethwaite and S. Olsen: 'An electrochemical model for prediction of corrosion of mild steel in aqueous carbon dioxide solutions', *CORROSION*, 1996, 52, 280–294.
9 F. Madani Sani, B. Brown and S. Nesic: 'An electrochemical study of the effect of high salt concentration on uniform corrosion of Carbon steel in aqueous CO₂ solutions', *J. Electrochem. Soc.*, 2021, 168, 051501.
10 G. Hinds, P. Cooling, A. Wain, S. Zhou and A. Turnbull: 'Technical note: measurement of pH in concentrated brines', *CORROSION*, 2009, 65, 635–638.
11 J. L. Crolet and M. R. Bonis: 'pH measurements in aqueous CO₂ solutions under high pressure and temperature', *Corrosion*, 1983, 39, 39–46.
12 H. Fang: 'Low temperature and high salt concentration effects on general CO₂ corrosion for carbon steel', Master's thesis, Ohio University, Athens, Ohio, 2006.
13 F. Madani Sani, B. Brown, Z. Belarbi and S. Nesic: in *CORROSION Conference*, Nashville, TN, NACE International, 2019, p. Paper No. 13026.
14 F. Madani Sani, B. Brown and S. Nesic: in *CORROSION Conference*, Virtual, NACE International, 2021, p. No. 16788.
15 R. D. Springer, P. Wang and A. Anderko: 'Modeling the properties of H₂S/CO₂/salt/water systems in wide ranges of temperature and pressure', *SPE J.*, 2015, 20, 1,120-1,134.
16 A. Kahyarian and S. Nesic: 'On the mechanism of carbon dioxide corrosion of mild steel: experimental investigation and mathematical modeling at elevated pressures and non-ideal solutions', *Corros. Sci.*, 2020, 173, 108719.

17 J. O. Bockris, D. Drazic and A. R. Despic: 'The electrode kinetics of the deposition and dissolution of iron', *Electrochimica Acta*, 1961, 4, 325–361.

18 R. J. Chin and K. Nobe: 'Electrodissolution kinetics of iron in chloride solutions III . acidic solutions', *J. Electrochem. Soc.*, 1972, 119, 1457–1461.

19 L. J. Vracar and D. M. Drazic: 'Influence of chloride ion adsorption on hydrogen evolution reaction on iron', *J. Electroanal. Chem.*, 1992, 339, 269–279.

20 D. G. Miller: 'Estimation of tracer diffusion coefficients of ions in aqueous solution', 1982, Lawrence Livermore Laboratory, University of California.

21 N. D. Pinto and E. E. Graham: 'Evaluation of diffusivities in electrolyte solutions using Stefan-Maxwell equations', *AIChE J.*, 1986, 32, 291–296.